

This work was written as part of one of the author's official duties as an Employee of the United States Government and is therefore a work of the United States Government. In accordance with 17 U.S.C. 105, no copyright protection is available for such works under U.S. Law.

Public Domain Mark 1.0

<https://creativecommons.org/publicdomain/mark/1.0/>

Access to this work was provided by the University of Maryland, Baltimore County (UMBC) ScholarWorks@UMBC digital repository on the Maryland Shared Open Access (MD-SOAR) platform.

**Please provide feedback**

Please support the ScholarWorks@UMBC repository by emailing [scholarworks-group@umbc.edu](mailto:scholarworks-group@umbc.edu) and telling us what having access to this work means to you and why it's important to you. Thank you.

## GRAVITATIONAL WAVES

# A gamma-ray pulsar timing array constrains the nanohertz gravitational wave background

The Fermi-LAT Collaboration\*†

After large galaxies merge, their central supermassive black holes are expected to form binary systems. Their orbital motion should generate a gravitational wave background (GWB) at nanohertz frequencies. Searches for this background use pulsar timing arrays, which perform long-term monitoring of millisecond pulsars at radio wavelengths. We used 12.5 years of Fermi Large Area Telescope data to form a gamma-ray pulsar timing array. Results from 35 bright gamma-ray pulsars place a 95% credible limit on the GWB characteristic strain of  $1.0 \times 10^{-14}$  at a frequency of  $1 \text{ year}^{-1}$ . The sensitivity is expected to scale with  $t_{\text{obs}}$ , the observing time span, as  $t_{\text{obs}}^{-13/6}$ . This direct measurement provides an independent probe of the GWB while offering a check on radio noise models.

Pulsars are spinning neutron stars that emit beams of broadband radiation from radio to gamma-ray wavelengths that appear to pulse as they periodically sweep across the line of sight to Earth (1). Millisecond pulsars (MSPs) spin at hundreds of hertz and pulse with sufficient regularity to function as celestial clocks, distributed across the sky and throughout the Galaxy. Timing of individual MSPs by use of radio telescopes has been used to test general relativity and alternative theories of gravity (2). Long-term monitoring campaigns of ensembles of MSPs are used to search for low-frequency gravitational waves (GWs), which are expected to be emitted by supermassive black hole (SMBH) binaries that are predicted to exist at the centers of galaxies that have undergone mergers. General relativity predicts that a circular binary with orbital frequency  $f/2$  will emit GWs with frequency  $f$  and amplitude  $\propto f^{2/3}$  (3). When SMBH binaries have an orbital separation of  $\sim 0.01 \text{ pc}$ , which is equivalent to  $\sim 2000$  astronomical units, the orbits decay primarily through GW emission. Because of this link between GW frequency and amplitude, the superposition of GWs from many SMBH binaries throughout the Universe is predicted to build up a GW background (GWB) with a characteristic GW strain  $h_c$  following a power law in frequency (4)

$$h_c(f) = A_{\text{gwb}} \left( \frac{f}{\text{year}^{-1}} \right)^\alpha \quad (1)$$

The spectral index  $\alpha$  is predicted to be  $-2/3$  for GW-driven binary inspirals, and the dimensionless strain amplitude  $A_{\text{gwb}}$  incorporates the growth, masses, and merger rates of SMBHs. If SMBHs do not rapidly migrate to the centers of newly merged galaxies, there

will be fewer wide binaries, reducing the GW power at low frequencies. Thus, the measured GWB is expected to carry information about the distribution of SMBH masses and the dynamical evolution of SMBH binary systems (5).

Searches for the GWB can be performed with ensembles of MSPs—known as pulsar timing arrays (PTAs) (6, 7)—by monitoring the times of arrival (TOAs) of the steady pulses from each pulsar, which arrive earlier or later than expected owing to the spacetime perturbations. Because the GWB is expected to be a sum of many individual sources, the induced

TOA variations are random and differ for each pulsar but have a common spectrum of power spectral densities,  $P(f)$

$$P(f) = \frac{A_{\text{gwb}}^2}{12\pi^2} \left( \frac{f}{\text{year}^{-1}} \right)^{-\Gamma} \text{ year}^{-3} \quad (2)$$

with spectral index  $\Gamma = 3 - 2\alpha = 13/3$  for SMBHs (4). This functional form has more power at low frequencies so is referred to as a red spectrum. For observations taken at an approximately fixed location (Earth), the GWB is expected to produce a signature quadrupolar pattern of TOA variations, known as the Hellings-Downs correlation (8).

Because the expected quadrupolar correlations are only about 10% of the total signal, the GWB is predicted to initially appear as a set of independent signals from each pulsar, with power spectra all consistent with Eq. 2. The quadrupolar distribution would only become evident in more sensitive observations. Radio PTAs have reported a red spectrum process with modest statistical significance (9–12), but no Hellings-Downs correlation has been found. These results could be compatible with  $\alpha = -2/3$  and  $A_{\text{gwb}} \sim 2 \times 10^{-15}$  to  $3 \times 10^{-15}$  at  $1 \text{ year}^{-1}$  (Fig. 1). This would be consistent with some predictions for the GWB (5), but because no spatial correlations have been detected, it could have other origins.

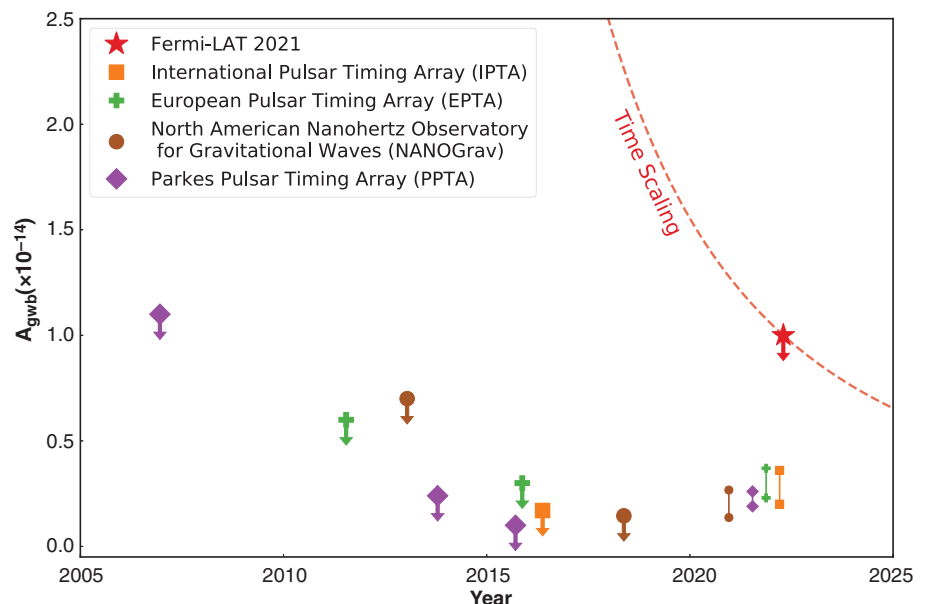


**Fig. 1. Constraints on the GW background from radio and gamma-ray PTAs.** The inferred constraints on the GWB amplitude at  $1 \text{ year}^{-1}$  ( $A_{\text{gwb}}$ ) are plotted as a function of publication date (data sources are listed in table S7) and assume  $\alpha = -2/3$ , as predicted for the superposition of GWs from merging black holes. Colored symbols correspond to each of the PTAs indicated in the key. Upper limits at 95% confidence are shown as downward arrows, and amplitude ranges indicate detections of a common noise process, which could be the GWB or have other origins. The Fermi-LAT 95% upper limit,  $1.0 \times 10^{-14}$ , uses data obtained up to January 2021 and is plotted at a publication date of April 2022. The dashed red line indicates the expected scaling of the Fermi-LAT limit as a function of time.

\*Fermi-LAT Collaboration authors and affiliations are listed in the supplementary materials.

†Corresponding authors: Matthew Kerr (matthew.kerr@gmail.com); Aditya Parthasarathy (adityapartha3112@gmail.com)

A potential alternative explanation for this signal is spin noise, which is approximately power-law red noise intrinsic to each pulsar, with some MSPs observed to have a spin noise spectral index ( $\Gamma$ ) of 2 to 7 (13, 14). Possible physical origins for spin noise include turbulence in the neutron star interior (15) and systematic variations in the magnetic field and corotating plasma, which govern the rotational energy loss of the pulsar (16). Pulsars that have spin noise spectra with similar shapes but different amplitudes—which is inconsistent with a GWB—could masquerade as a common mode signal without a Hellings-Downs correlation (10).

Another potential noise source for radio PTAs is the frequency-dependent effect of radio propagation through plasma, including the solar wind and the ionized interstellar medium (IISM). Pulsed radio emission at frequency  $\nu$  is delayed by time  $\tau_{\text{DM}}$

$$\tau_{\text{DM}} = 4.15 \text{ ms} \times \left( \frac{\text{DM cm}^3}{\text{pc}} \right) \times \left( \frac{\nu}{\text{GHz}} \right)^{-2} \quad (3)$$

where DM is the dispersion measure, equal to the total electron column density. The DM of a pulsar can vary with time because of the relative motions of Earth and the pulsar. Correcting for this effect requires repeated measurements by use of multifrequency radio observations and the introduction of many additional degrees of freedom to timing models. Because the propagation paths of radio waves through the IISM depend on  $\nu$ , the DM itself is frequency dependent (17, 18), so some of this delay is intrinsically unmeasurable. Other propagation effects include a broadening of the pulse, which can only be corrected for bright pulsars, with some components also being unmeasurable (19). Because the IISM is turbulent, these uncorrected delays introduce additional red noise to radio pulsar timing data. The variable solar wind introduces similar dispersive delays that can in principle be measured like DM variations but are only partially included in current models (20). Because of the wide angular extent of the solar wind, uncorrected delays would be correlated among pulsars. As with spin noise, IISM-induced noise with similar spectra could mimic a GWB signal. Predicted noise amplitudes are similar to the expected GWB signal, but these predictions rely on assumptions about the turbulent spectra of the IISM, which are poorly constrained by data (19). Further discussion of the modeling and impact of noise is available in (21).

Gamma-ray observations offer a potentially complementary approach: The much higher photon frequency means that the effects of the IISM and solar wind are negligible. The Large Area Telescope (LAT) (22), on the Fermi Gamma-ray Space Telescope, is sensitive to

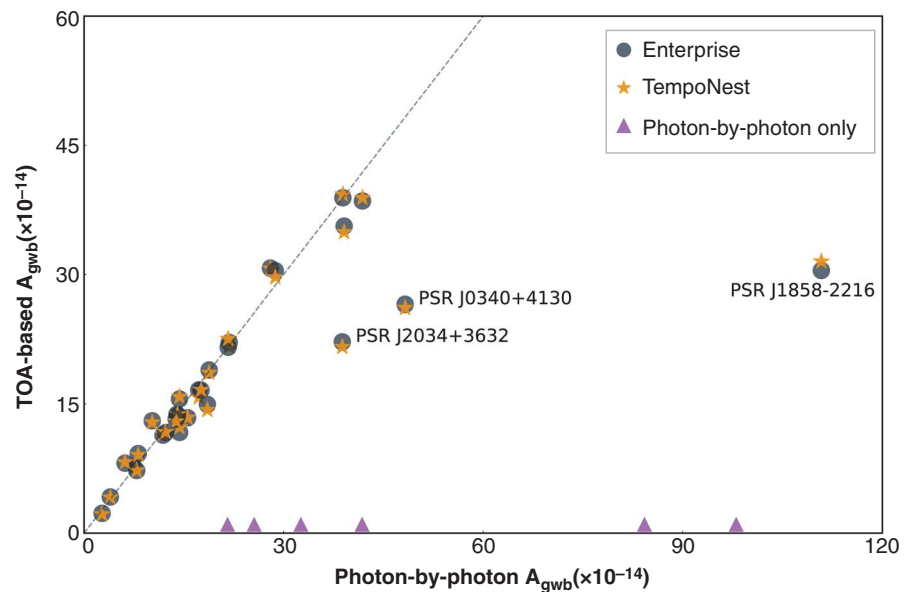


**Fig. 2. Comparison between  $A_{\text{gwb}}$  measurements from each pulsar by using three analysis methods.** Data points indicate the limits on an  $\alpha = -2/3$  GWB for 35 MSPs computed with three methods: Two TOA-based codes, TEMPONEST (orange stars) and ENTERPRISE (gray circles), are shown as a function of the limit from a photon-by-photon analysis (x axis). The dashed line indicates equality between the results of the TOA-based and photon-by-photon methods. Six pulsars (purple triangles) have only a photon-based analysis so are plotted arbitrarily at zero on the y axis. The three labeled pulsars are outliers (21).

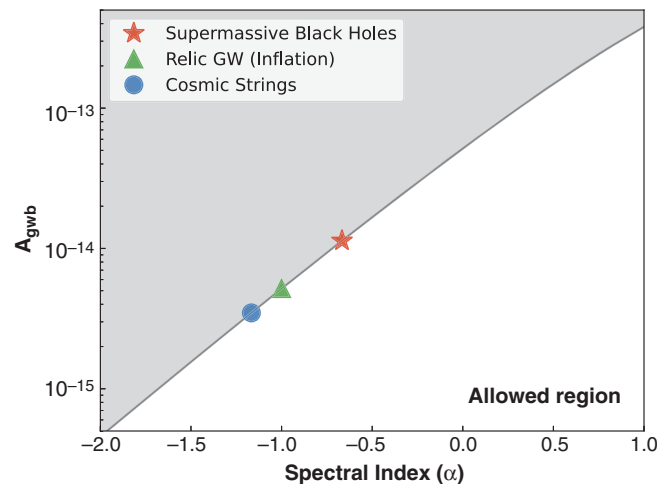


**Fig. 3. Gamma-ray constraints on different types of GWB sources.** GWB amplitudes  $A_{\text{gwb}}$  for assumed spectral indices  $\alpha$  in the shaded region are excluded with 95% confidence. The symbols indicate the values of  $\alpha$  expected for SMBH binaries (red star; our fiducial result), GWs generated during cosmic inflation (green triangle), and from hypothetical cosmic strings (blue circle).

giga-electron volt gamma-ray photons emitted by MSPs. Its 2.4-sr field of view performs a continuous survey, covering the full sky every two orbits (~3 hours). Its GPS clock records photon arrival times with <300 ns precision (23), enabling pulsar timing. Analyses of LAT survey data have detected 127 of the more than 400 known MSPs in the Milky Way (21, 24). The number of MSPs in this sample, long observing span, and instrumental stability enable a gamma-ray PTA whose characterization of spin noise and a potential GWB signal is free from IISM effects.

Using the 35 brightest and most stable gamma-ray MSPs and 12.5 years of Fermi-

LAT data, we searched for the GWB using two different techniques (21). First, we implemented a coherent photon-by-photon analysis that retains <1  $\mu\text{s}$  resolution. Second, for analysis with established software used for radio PTAs, we directly measured TOAs from the LAT data (25). Because the TOA estimation procedure requires averaging up to 1 year of data, this method loses sensitivity to signals with shorter time scales, and only 29 of the 35 pulsars are suitable.

For each pulsar, we searched for spin noise and derived an upper limit on  $A_{\text{gwb}}$  using (i) the photon-by-photon method and (ii) two TOA-based software packages, TEMPONEST

(26) and ENTERPRISE (27). None of the pulsars show evidence for spin noise (21), and the three different methods provide consistent results for each pulsar (Fig. 2), except in three cases (27).

Three of the pulsars in our sample have spin noise measurements from radio PTAs. Using the power spectral indices  $\Gamma$  measured from the radio timing data, we calculated 95% upper limits on spin noise amplitudes from the gamma-ray data. Our limits are below the previously measured values for PSR J0030+0451 (10% of the measured value) and PSR J1939+2134 (60 to 70%) but are unconstraining for PSR J0613-0200. This discrepancy might indicate contamination by residual IISM effects on the radio-based spin noise and GWB signal measurements. We combined the single pulsars into a PTA and estimated  $A_{\text{gwb}}$  limits under a variety of scenarios, including marginalization over possible spin noise and uncertainties in the position of Earth relative to the Solar System barycenter, and both excluding and including the expected Hellings-Downs quadrupolar spatial correlations (27). The resulting representative 95% confidence limit is  $A_{\text{gwb}} < 1.0 \times 10^{-14}$  (Fig. 1), a factor of 3 to 5 greater than the red spectrum process detected by radio PTAs.

For an idealized PTA, when a potential GWB signal is weak compared with other noise, the signal-to-noise ratio grows proportionally to  $A_{\text{gwb}}^2 \times t_{\text{obs}}^{\Gamma}$  (28, 29), where  $t_{\text{obs}}$  is the observing time span and  $\Gamma = 13/3$  for SMBHs, as in Eq. 2. This means that upper limits on  $A_{\text{gwb}}$  improve following the relation  $A_{\text{gwb}} \propto t_{\text{obs}}^{-13/6}$ . However, if the signal detected by radio PTAs does arise from the GWB, then these PTAs are now in the strong signal regime, and their sensitivity will improve more slowly ( $\propto t_{\text{obs}}^{-1/2}$ ). The differing time scalings and noise sources allow the gamma-ray PTA data to distinguish residual IISM variations from a potential GWB signal.

The Fermi PTA data have an essentially constant experimental setup; the data are almost uninterrupted, and calibrations have been constant for the full 12.5-year dataset. Gamma-ray data are potentially less subject to astrophysical effects, such as changes in the radio pulse shape (21). This stability is particularly useful for probing GWs with frequencies below  $0.1 \text{ year}^{-1}$ . Such low frequencies are predicted to constrain

the spectral shape of the GWB, which contains information about the physical sources (5).

There are other potential sources of power-law GWBs with different spectral indices,  $\alpha$ , such as  $\alpha = -1$  for relic GWs originating during scale-invariant inflation in the early Universe (30). Decay of (hypothetical) cosmic strings could also produce power-law spectra under a variety of scenarios (31). To constrain such sources, we computed corresponding 95% upper limits on  $A_{\text{gwb}}$  at different values of  $\alpha$  (Fig. 3). Other models are not well described by power laws, but their largest predicted signals are in or near the PTA band (32, 33).

We have used the Fermi-LAT dataset to construct a gamma-ray PTA. This provides an independent method to search for signals detected with radio PTAs. Unlike the radio PTAs, this method is free from the effects of the IISM. Most of the pulsars are amenable to the TOA-based approach, and the resulting datasets are small compared with those of radio PTAs, enabling analysis alongside radio PTA data with little additional computational burden.

## REFERENCES AND NOTES

1. A. Hewish, S. J. Bell, J. D. H. Pilkington, P. F. Scott, R. A. Collins, *Nature* **217**, 709–713 (1968).
2. C. M. Will, *Living Rev. Relativ.* **17**, 4 (2014).
3. B. P. Abbott et al., *Ann. Phys.* **529**, 1600209 (2017).
4. A. Sesana, F. Haardt, P. Madau, M. Volonteri, *Astrophys. J.* **611**, 623–632 (2004).
5. S. Burke-Spolaor et al., *Astron. Astrophys. Rev.* **27**, 5 (2019).
6. M. V. Sazhin, *Sov. Astron.* **22**, 36 (1978).
7. S. Detweiler, *Astrophys. J.* **234**, 1100 (1979).
8. R. W. Hellings, G. S. Downs, *Astrophys. J.* **265**, L39 (1983).
9. Z. Arzoumanian et al., *Astrophys. J.* **905**, L34 (2020).
10. B. Goncharov et al., *Astrophys. J. Lett.* **917**, L19 (2021).
11. S. Chen et al., *Mon. Not. R. Astron. Soc.* **508**, 4970–4993 (2021).
12. J. Antoniadis et al., *Mon. Not. R. Astron. Soc.* **510**, 4873–4887 (2022).
13. M. F. Alam et al., *Astrophys. J. Suppl. Ser.* **252**, 4 (2021).
14. B. Goncharov et al., *Mon. Not. R. Astron. Soc.* **502**, 478–493 (2021).
15. A. Melatos, B. Link, *Mon. Not. R. Astron. Soc.* **437**, 21–31 (2014).
16. A. Lyne, G. Hobbs, M. Kramer, I. Stairs, B. Stappers, *Science* **329**, 408–412 (2010).
17. J. M. Cordes, R. M. Shannon, D. R. Stinebring, *Astrophys. J.* **817**, 16 (2016).
18. J. Y. Donner et al., *Astron. Astrophys.* **644**, A153 (2020).
19. R. M. Shannon, J. M. Cordes, *Mon. Not. R. Astron. Soc.* **464**, 2075–2089 (2017).
20. C. Tiburzi et al., *Astron. Astrophys.* **647**, A84 (2021).
21. Materials and methods are available as supplementary materials.
22. W. B. Atwood et al., *Astrophys. J.* **697**, 1071–1102 (2009).
23. M. Ajello et al., *Astrophys. J. Suppl. Ser.* **256**, 12 (2021).
24. D. A. Smith et al., *Astrophys. J.* **871**, 78 (2019).
25. M. Kerr, P. S. Ray, S. Johnston, R. M. Shannon, F. Camilo, *Astrophys. J.* **814**, 128 (2015).
26. L. Lentati et al., *Mon. Not. R. Astron. Soc.* **437**, 3004–3023 (2014).
27. J. Ellis, M. Vallisneri, S. R. Taylor, P. T. Baker, ENTERPRISE: Enhanced Numerical Toolbox Enabling a Robust Pulsar Inference Suite, *Zenodo* (2020); doi: 10.5281/zenodo.4059815.
28. X. Siemens, J. Ellis, F. Jenet, J. D. Romano, *Class. Quantum Gravity* **30**, 224015 (2013).
29. N. S. Pol et al., *Astrophys. J. Lett.* **911**, L34 (2021).
30. W. Zhao, *Phys. Rev. D Part. Fields Grav. Cosmol.* **83**, 104021 (2011).
31. T. Damour, A. Vilenkin, *Phys. Rev. D Part. Fields Grav. Cosmol.* **71**, 063510 (2005).
32. Z. Arzoumanian et al., *Phys. Rev. Lett.* **127**, 251302 (2021).
33. A. Khmelnitsky, V. Rubakov, *J. Cosmol. Astropart. Phys.* **2014**, 019 (2014).
34. M. Kerr, A. Parthasarathy, Software and data release for Fermi Pulsar Timing Array, *Zenodo* (2022).

## ACKNOWLEDGMENTS

We dedicate this work to our recently deceased colleague, Jing Luo. We are grateful to the three insightful anonymous reviewers and to D. Champion for comments on an early draft. The Fermi-LAT Collaboration acknowledges support for LAT development, operation, and data analysis from NASA and the US Department of Energy (DOE) (United States); CEA/Irfu and IN2P3/CNRS (France); ASI and INFN (Italy); MEXT, KEK, and JAXA (Japan); and the K. A. Wallenberg Foundation, the Swedish Research Council, and the National Space Board (Sweden). Science analysis support in the operations phase from INAF (Italy) and CNES (France) is also gratefully acknowledged. The National Radio Astronomy Observatory is a facility of the National Science Foundation operated under cooperative agreement by Associated Universities. Pulsar research at UBC is supported by an NSERC Discovery Grant and by CIFAR. Work at NRL is supported by NASA. **Funding:** This work was performed in part under DOE contract DE-AC02-76SF00515. M.K. is supported by NASA grant NNG210B03A. E.C.F. and N.M. are supported by NASA under award 80GSFC21M0002. T.C. is supported by NASA through the NASA Hubble Fellowship Program grant HST-HF2-51453.001. K.C. is supported by a UBC Four Year Fellowship (6456). S.M.R. is a CIFAR Fellow and is supported by the NSF Physics Frontiers Center award 1430284. The work of M.A.S.C. and V.G. was supported by grants PGC2018-095161-B-I00 and CEX2020-001007-S, both funded by MCIN/AEI/10.13039/501100011033 and by ERDF. V.G. has been supported by Juan de la Cierva-Incorporación IJC2019-040315-I grants. G.Z. acknowledges financial support from the Slovenian Research Agency (grants P1-0031, I0-0033, and J1-1700). C.J.C. acknowledges support from the ERC under the European Union's Horizon 2020 research and innovation programme (grant agreement 715051; Spiders). S.J.S. holds an NRC Research Associateship award at NRL. **Author contributions:** M.K. conceived the project, implemented the gamma-ray analysis, and cowrote the manuscript. A.P. implemented the TOA-based analysis and cowrote the manuscript. D.A.S., P.S.R., M.P.R., and M.K. internally reviewed the manuscript. B.B., I.C., H.C., K.C., L.G., M.J.K., S.M.R., J.R., R.S., I.S., S.T., and G.T. contributed radio timing solutions. Other coauthors acquired Fermi-LAT data and reviewed and contributed to the manuscript. **Competing interests:** The authors declare that they have no competing interests. **Data and materials availability:** All raw data, processed data, reduced data, pulsar timing solutions, and software developed for this work are available on Zenodo (34).

## SUPPLEMENTARY MATERIALS

science.org/doi/10.1126/science.abm3231  
Fermi-LAT Collaboration Authors  
Materials and Methods  
Figs. S1 to S3  
Tables S1 to S8  
References (35–92)

10 September 2021; accepted 24 March 2022  
Published online 7 April 2022  
10.1126/science.abm3231

## A gamma-ray pulsar timing array constrains the nanohertz gravitational wave background

*Science*, 376 (6592), • DOI: 10.1126/science.abm3231

### A gamma-ray pulsar timing array

After galaxies merge, the supermassive black holes (SMBHs) at their centers are expected to form binaries that emit gravitational waves at nanohertz frequencies. Numerous SMBH binaries throughout the Universe should combine to produce a gravitational wave background. Existing searches for this signal use radio observations of pulsars as sensitive clocks and look for small shifts in the pulse timings. The Fermi-LAT Collaboration implemented a pulsar timing array using gamma rays and achieved a sensitivity close to that of the radio approaches. The results set an independent upper limit on the gravitational wave background, which is subject to different noise sources. —KTS

### View the article online

<https://www.science.org/doi/10.1126/science.abm3231>

### Permissions

<https://www.science.org/help/reprints-and-permissions>

Use of this article is subject to the [Terms of service](#)

*Science* (ISSN ) is published by the American Association for the Advancement of Science. 1200 New York Avenue NW, Washington, DC 20005. The title *Science* is a registered trademark of AAAS.

Copyright © 2022 The Authors, some rights reserved; exclusive licensee American Association for the Advancement of Science. No claim to original U.S. Government Works